Detailed structural analysis of epitaxial MBE-grown Fe/Cr superlattices by x-ray diffraction and transmission-electron spectroscopy

M. E. Gómez,[1,*] J. Santamaria,[1,†] S. Kim,[1] Kannan M. Krishnan,[2] and Ivan K. Schuller[1]

[1]*Department of Physics, University of California–San Diego, La Jolla, California 92093-0319, USA*
[2]*Department of Materials Sciences, University of Washington, Seattle, Washington 98195-2120, USA*

We have performed a detailed quantitative structural analysis of epitaxial $[\mathrm{Fe}(3\,\mathrm{nm})/\mathrm{Cr}(1.2\,\mathrm{nm})]_{20}$ superlattices by low- and high-angle x-ray diffraction, and energy-filtered transmission electron microscopy on cross-section samples. The interface roughness was changed systematically by varying the substrate temperature (150-250 °C) maintaining all other growth parameters fixed. Direct imaging of the interfaces allows examining the roughness of the individual interfaces and its evolution with thickness. A statistical analysis of the local interface width for the individual layers supplies the roughness static and dynamic exponents. High-temperature samples (250 °C) show roughness decreasing with thickness as a result of surface-diffusion-dominated growth. Low-temperature samples (150 °C) show anomalous non-self-affine roughness characterized by a time-dependent local interface width.

I. INTRODUCTION

Surface and interface roughness and its propagation in thin films and superlattices has been a subject of intense investigation in recent years not only to understand the basic laws governing film growth[1] but also to examine the influence of surface and interface disorder on the physical properties.[2] For single films, extensive experimental and theoretical work has shown that kinetic roughening follows frequently relatively simple scaling laws (*self-affine roughness*).[1] In-self affine surfaces of size L, the roughness frequently follows the Family-Vicsek dynamic scaling,[3] in which the local $[\sigma(l,t)]$ and global $[\sigma(L,t)]$ height fluctuations scale with the same roughness exponent α $[\sigma(l,t) \propto l^\alpha; \sigma(L,t) \propto L^\alpha]$. For superlattices the situation is considerably more complex. On the one hand, the access to the buried interfaces is experimentally difficult, and on the other hand roughness evolution may be complicated by having more than one constituent. In a recent Letter[4] we have reported a study of interface disorder and its evolution with thickness for Fe/Cr superlattices grown by dc sputtering. A statistical analysis of the height distribution of the individual interfaces obtained by energy-filtered transmission electron microscopy (EFTEM) provided experimental evidence for non-self-affine anomalous roughness.[5,6] For anomalous scaling, the roughness exponents at short (α_{loc}) and long length scales (α) are different and the local interface width is no longer time independent at short distances (as in the Family-Viseck ansatz[3]), but it follows a power law with a new exponent β_{loc}.[5,6] We found[4] that for sputtered Fe/Cr superlattices static and dynamic roughness exponents do not fit in any of the existing model classes of surface growth that are known to exhibit anomalous scaling. These models involve exclusively surfaces grown by an idealized molecular beam epitaxy (MBE) which are claimed to be simpler to treat theoretically than those grown by sputtering. On the other hand, to the best of our knowledge, the only experimental reports of anomalous scaling in thin films[7] and superlattices[4] involve polycrystalline samples grown by electrodeposition or sputtering (not MBE). MBE growth models deal with local growth processes, for which the growth rate depends on the local properties of the interface. However there are a number of systems, like sputter growth, for which *nonlocal* effects contribute to the interface morphology and growth velocity. Sputter deposition is influenced by nonlocal effects due to geometrical shadowing, i.e., the local growth rate at a given point is proportional to its exposure to the deposition flow. The question arises then, to what extent anomalous scaling and/or the values of the scaling exponents are determined by the growth technique. In this paper we examine this issue on MBE-grown Fe/Cr superlattices.

We have grown Fe/Cr superlattices by MBE changing systematically the interface roughness by controlling substrate temperature during growth, maintaining all the other growth parameters constant. We characterize the interfacial structure with the combined use of x-ray diffraction (XRD) and transmission electron microscopy. XRD provides averaged structural information on lattice parameters, modulation lengths, and disorder averaged over the whole superlattice stack. Extracting quantitative information on the interface structure (averaged roughness) requires fitting diffraction spectra to structural models ("refinement"). This we have done quite successfully for different superlattices using the SUPREX refinement method.[8] Concerning microscopy, since Fe and Cr have similar lattice parameters and exhibit very close elastic scattering factors for electrons, conventional diffraction contrast and/or phase contrast imaging in a TEM resolve neither the layers nor the details of their interface structure. To overcome this problem analytical tools, such as energy filtered transmission electron microscopy, are necessary, which give specific chemical information with spatial resolution at nanometer scale.[9,10] Statistical analysis of the digitized images allows probing directly the roughness for each layer, its lateral length scale, and replication from layer to layer. Complementary information is obtained about short scale range roughness based on the analysis of the reflection

high-energy electron diffraction (RHEED) intensity profile, which was taken *in situ* during the MBE growth.

II. EXPERIMENT

Epitaxial Fe/Cr superlattices sandwiched between bottom and top (100 nm) Nb layers were grown on *r*-plane-oriented sapphire substrates. Samples with 20 bilayers, Fe (3 nm)/Cr (1.2 nm), were grown by MBE with substrate temperature ranging between 150 and 250 °C. The 100 nm Nb layers were always grown under the same conditions and with the same thickness for all samples to ensure that the Nb buffer layer had always the same roughness.

The superlattice structure was thoroughly characterized by low-angle x-ray diffraction using a rotating anode diffractometer with Cu $K\alpha$ radiation. To estimate the interfacial roughness of the layers, the specular reflectivity spectra were analyzed with the SUPREX refinement program,[8] in which the roughness was assumed to replicate from layer to layer according to a power law $\sigma_n = \sigma_a n^\alpha$, where σ_a is the roughness of the first bilayer, n is the layer index, and α an exponent describing the roughness evolution from layer to layer.

Electron microscopy was carried out using a Philips CM20-FEG TEM equipped with a Gatan Imaging Filter, capable of obtaining both electron energy-loss spectra (EELS) and energy-filtered images in real time at high spatial resolution.[9,10] The electron energy-loss spectroscopy offers better spatial resolution than other analytical tools such as EDX. Samples suitable for imaging by TEM were prepared in the cross-section geometry following customary treatment of polishing, dimpling, and low-angle (less than 10°) ion milling to get large electron-transparent regions thin enough for EELS investigations without any multiple scattering. Energy-filtered imaging techniques (after removal of the background due to other loss processes) were carried out on cross-sectional images to show the Fe or Cr elemental maps at sufficient resolution to quantify the local structural roughness at the Fe/Cr or Cr/Fe interfaces, as described elsewhere. The digitized images were analyzed with help of the Gatan Digital Micrograph software to obtain Cr-Fe profiles, integrating the intensity over windows 0.27 nm wide centered around points separated by 1.35 nm. Since Cr and Fe profiles for the same bilayers were nearly identical, we will here after assume that the bilayer composition profile describes the interface.[11]

III. RESULTS

A. X-ray diffraction

Figure 1 shows typical low-angle x-ray spectra for Nb(100 nm) [Fe(3 nm)/Cr(1.3 nm)]$_{20}$Nb(100 nm) superlattices grown at substrate temperature (T_S) ranging between 150 and 300 °C. Their refinement using the SUPREX program[8] (also shown in Fig. 1) allows determination of structural parameters. Qualitatively the roughness increases rapidly with decreasing temperature as observed from the reduction of the intensity of the superlattice peaks at 2θ = 2.2 and 4.3. The Nb base and capping layer have a major influence on the low-angle diffraction spectra complicating
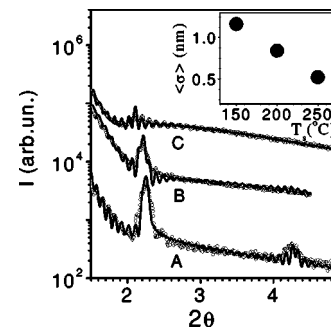
FIG. 1. Low-angle x-ray diffraction spectra for superlattices grown at different substrate temperatures T_S. A, 250 °C; B, 200 °C; C, 150 °C. The inset shows temperature dependence of the average roughness $\langle \sigma \rangle$.

the refinement procedure considerably. To arrive at meaningful initial values of the input parameters for the refinement process, we performed a systematic study by varying the Nb buffer layer thickness. We grew a series of samples with 20 Fe/Cr bilayers changing the Nb buffer layer thickness between 10 and 100 nm. The low-angle x-ray diffraction (XRD) patterns for [Fe(3nm)/Cr(1.3nm)]$_{20}$ superlattices grown at 250 °C varying the Nb buffer layer thickness are shown in Fig. 2. Open circles correspond to the experimental data; the lines are obtained from the SUPREX program.[8] This allows understanding the evolution of the low-angle spectra with base Nb thickness. In addition to the superlattice peaks two modulations are present, a long wavelength corresponding to the Nb buffer layer which becomes shorter when increasing the buffer thickness. As the buffer layer thickness becomes comparable to the superlattice layer thickness, interference effects arise which may complicate the refinement considerably. In this way it is possible to arrive at meaningful roughness values from the x-ray data of Fig. 1. Typical roughness values for the 100 nm Nb buffer layer were between 1.5 and 2.5 nm. The averaged roughness for the superlattices is displayed in the inset of Fig. 1. It should be noted that the roughness influences not only the sharpness of the superlattice peaks but also the intensity profile at very low angles. Once we are able to refine the structure including the Nb buffer layer, the sensitivity to the superlattice roughness can be addressed. To this end, we address two separate
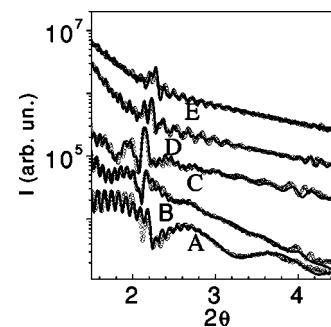
FIG. 2. Low-angle x-ray diffraction spectra of [Fe(3 nm)/Cr(1.3 nm)]$_{20}$ superlattices grown at 250 °C with A, 9 nm; B, 19 nm; C, 29 nm; D, 56 nm; E, 85 nm Nb buffer layer. Lines are refinements using the SUPREX program.
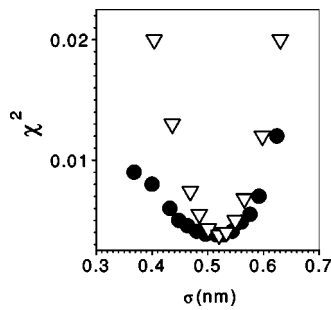
FIG. 3. Sensitivity of the refinement (χ^2) to the average roughness of the superlattice when different roughness values were fixed and the remaining parameters allowed to vary (solid circles) or when the roughness was changed manually keeping all the remaining parameters fixed (open triangles).

issues. Sensitivity of the refinement to this roughness value was checked by examining the evolution of the quality factor of the fit, χ^2. We changed the roughness step by step keeping all other parameters fixed and using χ^2 as an indicator of the refinement quality. Figure 3 (down triangles) shows that χ^2 as a function of roughness σ_a displays a sharp minimum showing the sensitivity of the refinement to this roughness. We also changed the roughness step by step and kept each value fixed while the remaining parameters were allowed to vary until χ^2 also shows a minimum (see circles in Fig. 3). The width of this shallower minimum provides an upper limit of 15% in the error of the roughness.

The high-angle diffraction spectra provide information about short length scale disorder like interface steps and interdiffusion, which results in a fluctuation in the layer thickness. High-angle diffraction spectra for Nb(100 nm)[Fe(3 nm)/Cr(1.3 nm)]$_{20}$Nb(100 nm) superlattices grown at different temperatures are shown in Fig. 4. The Nb diffraction peak close to 39° overlaps with the Fe/Cr (100) superlattice peaks centered around 44.7°. Even for very thin Nb buffer layers there is significant overlap, thus altering the intensity profile of the superlattice peak. The sharpness of the superlattice satellites at the right-hand side of the superlattice Bragg peak changes with temperature, reflecting a larger amount of step disorder for samples grown at high temperature. The overlap problem was avoided by
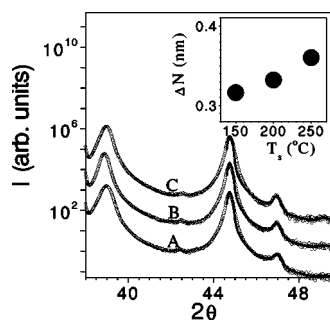
FIG. 4. High angle x-ray diffraction spectra of superlattices grown at different temperatures: 250 °C (*A*), 200 °C (*B*), 150 °C (*C*). Lines are the refinements using the SUPREX program. Inset shows the temperature dependence of the bilayer thickness fluctuations $\triangle N$.
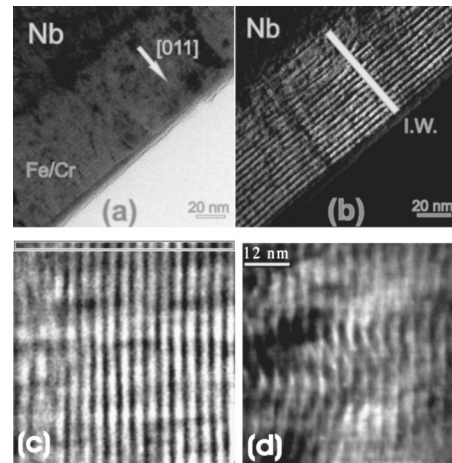
FIG. 5. (a) Transmission electron micrograph of a Fe/Cr multilayer grown on a niobium buffer layer. (b) Typical energy-filtered transmission electron Fe map of Nb(100 nm)[Fe(3 nm)/Cr(1.2 nm)]$_{20}$ multilayer at low magnification. (c) High-magnification EFTEM maps for quantitative roughness evaluation of samples grown at 250 (c) and 150 °C (d).

fitting only the right side of the superlattice peak when Nb layers were present. Due to the limited fitting range we were not able to resolve the contribution of the individual layers to the bilayer thickness fluctuation, i.e., the same quality of the fit is obtained when the roughnesses of the two elements are exchanged, or when the whole roughness is assigned to one of them. The fitted average bilayer thickness fluctuations ΔN are collected in the inset of Fig. 4 showing that step disorder increases monotonically with temperature. A comparison of the high- and low-angle results implies that the interdiffusion increases with temperature (from high angle), i.e., the sample becomes rougher at short length scales but smooths at long length scales as indicated by the low-angle scattering.

B. EFTEM analysis

A conventional low-magnification cross-sectional TEM bright field image of a typical Nb(100 nm)/[Fe(3 nm)/Cr(1.3 nm)]$_{20}$/Nb(100 nm) multilayer grown at a substrate temperature of 250 °C is shown in Fig. 5(a). The diffraction contrast allows the identification of the different layers in the structure (Nb base layer, Fe-Cr superlattices, and the Nb capping layer) and reveals columnar microstructure, in all three layers. The energy-filtered imaging technique was applied to infer elemental maps from the multilayered specimen. A typical low magnification EFTEM map in cross-section view of an [Fe(3 nm)/Cr(1.2 nm)]$_{20}$ superlattice is shown in Fig. 5(b). The bright intensity is proportional to the intensity of the Fe-characteristic $L_{2,3}$ energy-loss signal; dark regions mean absence of Fe. In contrast to the micrograph shown in Fig. 5(a), the Fe and Cr layers are clearly separated. Figures 5(c) and 5(d) show high-magnification EFTEM plots for quantitative roughness evaluation of samples grown at 250 and 150 °C, respectively. The low-temperature sample (150 °C) is considerably rougher than the high-temperature one (250 °C). EFTEM composition maps were digitized with
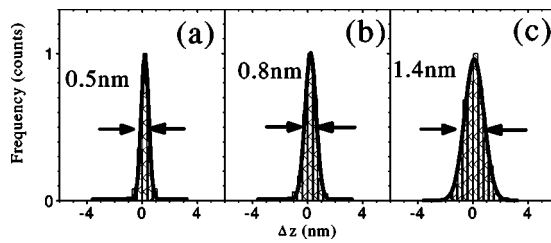
FIG. 6. Histogram of height differences of interface points spaced $R=4$ nm. Different histograms correspond to different growth temperatures: 150 (a) 200 (b), and 250 °C (c). Arrows show the full width at half maximum, and the corresponding values are written in each plot.

the help of the Gatan Digital Micrograph software. Digitized layer profiles can be statistically analyzed to obtain the layer profile $h_n(x,t)$ for each layer n, as described in detail elsewhere.[11–13] These profiles can be statistically analyzed to examine the nature of the roughness and its propagation properties.

The first interesting observation is that the distribution of height differences for each bilayer $h_n(x+l,t)-h_n(x,t)$ is Gaussian with a standard deviation $\langle[h_n(x+l,t)-h_n(x,t)]^2\rangle$ increasing with the distance between points, l, up to a saturation value. This height-height correlation function $g(l,t) \equiv \langle[h(x+l,t)-h(x,t)]^2\rangle$ is customarily analyzed to describe roughness evolution. The Gaussian nature of the roughness is a central assumption made in diffuse XRD experiments to quantitatively analyze roughness.[14–17] Our EFTEM digitized multilayer maps provide a direct proof of the random Gaussian distribution of height differences for the individual bilayers. The local interface width $\sigma(l,t)=[\langle z_n^2(x,t)\rangle]^{1/2}$ was also analyzed for the individual bilayers in terms of the standard deviation of the height distribution $z_n(x,t)=h_n(x,t)-\langle h_n(x,t)\rangle$. Note that averages are done over a window width l around each point. This distribution was also found to be Gaussian. Figures 6(a)–6(c) plot the statistical distribution of the heights $z(x)$ for samples grown at different temperature. They show a decrease of the full width at half maximum (FWHM) with increasing growth temperature, indicating that the sample grown at the highest temperature has the lowest roughness. Both pictures are equivalent, since, as shown by numerical simulations $g(l,t)/\propto\sigma(l,t)$.[1] In the following roughness is described in terms of the local interface width $\sigma(l,t)=[\langle z_n^2(x,t)\rangle]^{1/2}$.

Figure 7 shows the local interface width as a function of the window width for the individual bilayers, for samples grown at 150 (a) and 250 °C (b). In the low-temperature sample [Fig. 7(a)] the roughness increases with lateral window size l according to a power law $(\alpha(l) \sim l^{\alpha_{loc}})$ and then saturates. The position of the "knee" at saturation is a measure of the lateral correlation length ξ of the roughness. ξ is extracted from fits of the size dependent roughness for each bilayer to the expression $\sigma_n(l)=\sigma_{s,n}\{1-\exp[-(l/\xi)^{2\alpha_{loc}}]\}^{1/2}$, where $\sigma_{s,n}$ is the saturation value of the roughness for bilayer n, and α is the roughness exponent.[17] The lines in Fig. 7(a) are fits to this expression, which has the asymptotic behavior $\sigma(l\ll\xi)\approx l^{\alpha_{loc}}$ and $\sigma(l>\xi)\approx\sigma_s$. The roughness exponent
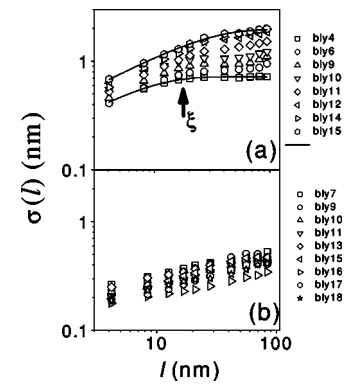
FIG. 7. Lateral evolution of the local interface width $\sigma(l)$ for the different bilayers for samples grown (a) at 150 and (b) at 250 °C. Different data sets correspond to different bilayers. Legends in the figures show the bilayer index (bly) for the different data sets. Lines are fits to $\sigma_n(l)=\sigma_{s,n}\{1-\exp[-(l/\xi)^{2\alpha_{loc}}]\}^{1/2}$ to obtain the roughness exponent α_{loc} and the lateral correlation length ξ.

α_{loc} was 0.56 ± 0.05 for the low-temperature sample. The high-temperature sample on the other hand shows smaller roughness and no indications of saturation, showing that the roughness lateral correlation length is larger than the lateral size of our images. Surprisingly, in this sample the roughness decreases with bilayer index, i.e., the interface becomes smoother when thickness increases.

The evolution of the roughness parameters with bilayer index can be used to obtain dynamic information of the growth provided the thickness increases linearly with time. The first observation is that for both samples the interface width $\sigma(l,t)$ depends on thickness (time) at small length scales. This is a first indication of non-self-affine anomalous scaling since as quoted in the Introduction, in self-affine interfaces the interface width at short length scale is time (thickness) independent. Figure 8 shows the thickness (time) dependence of $\xi(t)$ [Fig. 8(a)] and of the saturation roughness $\sigma_s(t)$ [Fig. 8(b), solid squares] for the low-temperature
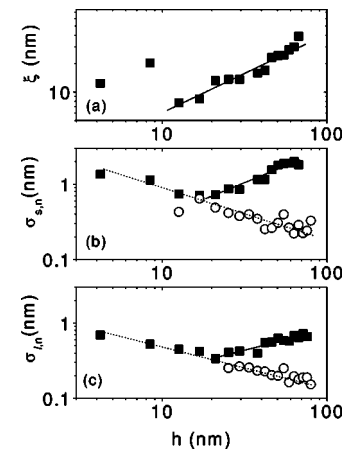
FIG. 8. (a) Thickness (time) dependence of the (a) lateral roughness correlation length for samples grown at 150 °C , (b) saturation interface width for samples grown at 150 (open circles) and 250 °C (solid squares), and (c) short range local interface width for samples grown at 150 (open circles) and 250 °C (solid squares).
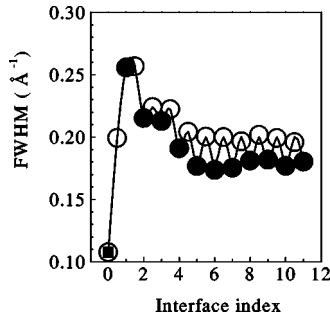
FIG. 9. FWHM of the (000) RHEED reflection for Fe (solid circles) and Cr (open circles) surfaces.

FIG. 10. Substrate temperature T_S dependence of the averaged saturation roughness $\langle\sigma_s\rangle$ obtained from the analysis of EFTEM images (open squares) and from x-ray refinement (open circles).

samples. For length scales larger than 15 nm both quantities show power law thickness dependence $[\sigma_s(t)\propto t^\beta;\ \xi(t)\propto t^{1/z}]$ with exponents $\beta=0.95\pm0.05$ and $1/z=0.83\pm0.05$. At short length scales saturation roughness decreases with thickness up to 15 nm. Since for the low-temperature sample ξ cannot be defined within our experimental window, we plot in Fig. 8(b) (open circles) the thickness dependence of the roughness at the largest length scale available from the EFTEM images. This long scale roughness decreases with thickness (bilayer index) as a power law with exponent $\beta=-0.73$. This can be directly observed by direct inspection of the EFTEM image of Fig. 5 for the first bilayers, and is also confirmed by RHEED for each interface. Figure 9 shows the FWHM of the RHEED (000) reflection as a function of bilayer index, for each element. The FWHMs of the Cr layers are always slightly larger than those for the Fe layer, indicating that the Cr layer grows more roughly on Fe than Fe on Cr, but a clear decrease in the overall FWHM is observed with bilayer index consistent with a decreasing roughness. Interestingly the decreasing saturation roughness of the low-temperature sample at short length scale seems to follow the same power law [see dotted line in Fig. 8(b)].

Figure 8(c) shows the short length scale roughness (interface slope) as a function of thickness (time) for low- (solid squares) and high- (open circles) temperature samples. The behavior is similar to that found for the saturation roughness but with smaller exponents. For the low-temperature sample $\log_{10}\sigma(l,t)$ is approximately linear with $\log_{10}(t)$ for length scales larger than 20 nm, with an exponent $\beta_{loc}=0.50\pm0.05$ [continuous line in Fig. 8(c)]. In this sample, roughness exponents determined independently were in good agreement with the relation $\alpha_{loc}=(\beta-\beta_{loc})z$, which holds for anomalous scaling .[5,6] Using $\alpha_{loc}=\alpha-\beta_{loc}z$ a global roughness exponent $\alpha=1.15\pm0.05$ was obtained. The high-temperature sample on the other hand shows a monotonic decrease of the interface slope with bilayer index with an exponent $\beta_{loc}=-0.5$ [dotted line of Fig. 8(c)].

It is worth noting that for both samples the saturation roughness (long length scale roughness for the high-temperature sample) averaged over the different bilayers was in good quantitative agreement with the values obtained from the refinement of specular low-angle XRD patterns. Figure 10 displays averaged roughness values obtained from x-ray diffraction (open circles) and EFTEM (open squares) showing the excellent agreement between both techniques.
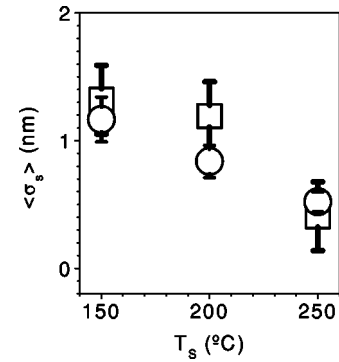
The saturation roughness of the first bilayer can be used to estimate the roughness of the Nb buffer layer: the value of 1.5 nm obtained from Fig. 8(c) is also in good agreement with the value obtained from the x-ray refinement.

IV. DISCUSSION

The decrease of the roughness with increasing thickness for the first Fe/Cr bilayers in the low-temperature sample and over the whole window for the high-temperature sample arise from surface diffusion on the growth process on the rough Nb buffer layer. Deposited atoms diffuse on the growing surface searching for the energetically most favorable positioning in a thermally activated process determined by the binding energies. Thus the motion of an atom on the surface depends on the number of bonds to be broken, and not on the interface height, as in random deposition models with surface relaxation, where atoms search for the lowest height position. The number of bonds an atom may form increases with the local curvature of the interface at that point.[1] If the local radius of curvature is positive the atom has a large number of neighbors and moving away from the site is difficult. On the other hand, if the radius of curvature of the surface is negative, the atom has fewer neighbors and diffuses more easily. Therefore in the high-temperature MBE growth on a rough surface, surface diffusion will result in the growing surface to smooth with thickness (as observed for the high-temperature sample). When the temperature is lowered the diffusion length decreases, atoms nucleate in islands, and the surface becomes rough, as found for the low-temperature sample for superlattice thickness larger than 15 nm. In addition, surface diffusion on a rough surface (Nb) will favor layer thickness fluctuations in a lateral length scale comparable to the diffusion length. This is probably the explanation of the larger superlattice period fluctuation found from x-ray analysis for the high-temperature sample despite its smaller overall roughness.

While in the high-temperature sample growth is dominated by surface diffusion and the interface roughness decreases with increasing thickness, the low-temperature sample shows an increase of the roughness with bilayer index following the scaling relations of anomalous scaling, as

TABLE I. Roughness scaling exponents for Fe/Cr superlattices grown by sputtering (Ref. 4) and by MBE together with the predicted exponents of MBE theories showing anomalous scaling.

crowth method	α_{loc}	β_{loc}	β	α	l/z
MBE ($T_S = 250$ °C)		-0.50 ± 0.50	-0.73 ± 0.05		
MBE ($T_S = 150$ °C)	0.55 ± 0.05	0.50 ± 0.05	0.95 ± 0.05	1.17 ± 0.05	0.83 ± 0.05
Sputtering (high pressure)	0.75 ± 0.05	0.22 ± 0.05	0.76 ± 0.05	1.05 ± 0.05	0.70 ± 0.05
Sputtering (low pressure)	0.65 ± 0.05	0.22 ± 0.05	0.25 ± 0.05		≈ 0
Linear MBE (Ref. 8)	1	1/8	3/8	1.5	0.25
Random diffusion (Ref. 9)	0.5			>0.5	<0.5
Nonlinear MBE (Ref. 10, 24)	0.73	1/11	1/3	1	0.33

found in our previous Letter[4] for sputtered samples. This allows discarding nonlocal effects related to sputter growth as the origin of the anomalous scaling. Moreover, the scaling exponents, although different from those found for sputtered superlattices, do not meet the predictions of any of the existing theories for surface growth exhibiting anomalous scaling: in the linear MBE model $\alpha = 3/2$, $\alpha_{loc} = 1$, $1/z = 0.25$;[18] in the random diffusion model[19] $\alpha_{loc} = 0.5$, $\alpha = 1/[2(1-\mu)]$ and $1/z = (1-\mu)/(2-\mu)$, where $1 < \mu < 0$ is a disorder-dependent parameter; and in discrete MBE models[20] based on the Lai–Das Sarma–Villain equation for MBE growth $\alpha = 1$, $\alpha_{loc} = 0.73$, $1/z = 0.33$.[21] For comparison we have gathered in Table I the scaling exponents of MBE superlattices (this work), sputtered superlattices (Ref. 4), and the exponents of MBE theories showing anomalous scaling. It is thus clear that anomalous scaling does not originate in the peculiarities of the growth process although they might influence the exponent values.

V. SUMMARY

In summary, we have analyzed quantitatively the interface roughness in MBE-grown Fe/Cr superlattices by XRD and EFTEM. We found that growth at high temperatures is dominated by surface diffusion while low substrate temperature results in island growth. We find evidence for anomalous non-self-affine scaling of the interface roughness in the low-temperature superlattices characterized by a time-dependent local roughness at short length scales with scaling exponents different from those previously found in sputtered superlattices. Our work constitutes a firm indication that anomalous scaling cannot be ascribed to the nonlocal effects characteristic of sputter growth. Future work will be directed to examine the connection of the roughness evolution with the magnetic and transport properties of these samples.

ACKNOWLEDGMENTS

---

*On leave from Universidad Del Valle, Cali, Colombia.

†On leave from Universidad Complutense de Madrid, Madrid, Spain.

[1] A. L. Barabasi and H. E. Stanley, *Fractal Concepts in Surface Growth* (Cambridge University Press, Cambridge, U.K., 1995).

[2] E. E. Fullerton, D. M. Kelly, J. Guimpel, I. K. Schuller, and Y. Bruynseraede, Phys. Rev. Lett. **68**, 859 (1992); J. Santamaria, M. E. Gómez, M. C. Cyrille, C. Leighton, K. M. Krishnan, and Ivan K. Schuller, Phys. Rev. B **65**, 012412 (2001).

[3] F. Family and T. Viseck, J. Phys. A **18**, L75 (1985).

[4] J. Santamaría, M. E. Gómez, J. L. Vicent, K. M. Krishnan, and Ivan K. Schuller, Phys. Rev. Lett. **89**, 190601 (2002)

[5] J. M. Lopez, Phys. Rev. Lett. **83**, 4594 (1999).

[6] J. J. Ramasco, J. M. Lopez, and M. A. Rodriguez, Phys. Rev. Lett. **84**, 2199 (2000).

[7] S. Huo and W. Schwarzacher, Phys. Rev. Lett. **86**, 256 (2001).

[8] I. K. Schuller, Phys. Rev. Lett. **44**, 1597 (1980); W. Sevenhans, M. Gijs, Y. Bruynseraede, H. Homma, and I. K. Schuller, Phys. Rev. B **34**, 5955 (1986); E. E. Fullerton, I. K. Schuller, H.

Vanderstraeten, and Y. Bruynseraede, *ibid.* **45**, 9292 (1992); D. M. Kelly, E. E. Fullerton, J. Santamaria, and I. K. Schuller, Scr. Metall. Mater. **33**, 1603 (1995).

[9] David B. Williams and C. Barry Carter, *Transmission Electron Microscopy IV Spectrometry* (Plenum Press, New York, 1996).

[10] R. F. Egerton, *Electron Energy Loss Spectroscopy* (Plenum Press, New York, 1996).

[11] M. E. Gómez, J. Santamaria, M. C. Cyrille, E. C. Nelson, Kannan M. Krishnan, and Ivan K. Schuller, Eur. Phys. J. B **30**, 17 (2002).

[12] M. C. Cyrille, S. Kim, M. E. Gómez, J. Santamaria, Kannan M. Krishnan, and Ivan K. Schuller, Phys. Rev. B **62**, 3361 (2000).

[13] M. C. Cyrille, S. Kim, M. E. Gómez, J. Santamaria, C. Leighton, Kannan M. Krishnan, and Ivan K. Schuller, Phys. Rev. B **62**, 15 079 (2000).

[14] T. Salditt, T. H. Metzger, and J. Peisl, Phys. Rev. Lett. **73**, 2228 (1994).

[15] R. Paniago, R. Forrest, P. C. Chow, S. C. Moss, S. S. P. Parkin, and D. Cookson, Phys. Rev. B **56**, 13 442 (1997).

[16] Y. H. Phang, D. E. Savage, R. Kariotis, and M. G. Lagally, J. Appl. Phys. **74**, 3181 (1993).

[17] S. K. Sinha, E. B. Sirota, S. Garoff, and H. B. Stanley, Phys. Rev. B **38**, 2297 (1988).

[18] J. G. Amar, P.-M. Lam, and F. Family, Phys. Rev. E **47**, 3242 (1997); S. Das Sarma, S. V. Ghaisas, and J. M. Kim, *ibid.* **49**, 122 (1994).

[19] J. M. Lopez and M. A. Rodriguez, Phys. Rev. E **54**, R2189 (1996).

[20] S. Das Sarma, S. J. Lanczycki, R. Kotlyar, and S. V. Ghaisas, Phys. Rev. E **53**, 359 (1996); C. Dasgupta, S. Das Sarma, and J. M. Kim, *ibid.* **54**, R4552 (1996).

[21] Z. W. Lai and S. Das Sarma, Phys. Rev. Lett. **66**, 2348 (1991); J. M. Kim and S. Das Sarma, *ibid.* **72**, 2903 (1994).